Bainitic transformation during the two-step Q&P process in a lean medium Mn steel containing silicon

S. Kaar, R. Schneider, D. Krizan, C. Béal, C. Sommitsch

Lean medium Mn Quenching and Partitioning (Q&P) steels with Mn contents up to 5 wt-% have recently gained a lot of interest due to their promising combination of strength and ductility. This steel group is characterized by a microstructure consisting of a carbon-depleted tempered martensitic (α'') matrix and a considerable amount of retained austenite (RA) stabilized by both, C and Mn, in order to ensure a sufficient strain-induced austenite to martensite transformation (TRIP-effect). Furthermore, the hard α'' matrix contributes to the excellent performance of these steels in bending, sheet cutting and hole expansion operations. In this contribution, the impact of the Q&P process on the transformation behavior of a 0.2C-4.5Mn-1.5Si lean medium Mn steel is presented and discussed in detail. This includes dilatometric experiments examining the influence of the Q&P process parameters on the phase transformations, light optical and scanning electron microstructural (LOM, SEM) investigations, as well as hardness measurements according to Vickers. Moreover, the Q&P annealing approach was compared to the TRIP-assisted bainitic ferrite (TBF) process, in order to evaluate the influence of primary martensite ($\alpha'_{initial}$) being present in the Q&P samples at the onset of isothermal bainitic transformation (IBT) on the transformation kinetics. With increasing quench temperature (T_Q) the amount of α" significantly decreased, whereas the phase fraction of bainitic ferrite (α_B) and RA continuously increased, leading to the formation of fresh martensite (α'_{final}) and the sharp decrease of the RA fraction at T_Q exceeding 250°C. Furthermore, with increasing partitioning temperature (T_P) a decreasing amount of α_B, associated with an increasing amount of α'_{final}, could be examined. The comparison of the Q&P and TBF process in terms of transformation behavior manifested a pronounced influence of the presence of $\alpha'_{initial}$, since the IBT was intensively accelerated in the Q&P samples.

KEYWORDS: MEDIUM MN STEEL - Q&P PROCESS - PHASE TRANSFORMATION - BAINITE - RETAINED AUSTENITE

Introduction

High demands on crash safety and environmental protection are driving factors for the application of new steel grades in the automotive industry. (1) Stringent requirements in terms of reducing CO_2 emissions, improving crashworthiness and enhancing the formability of complex shaped parts are impelling motives for the steel industry to the development of Advanced High Strength Steels (AHSS) (2,3). By the application of AHSS grades, the sheet thick-

Simone Kaar, Reinhold Schneider
University of Applied Sciences Upper Austria, Austria

Daniel Krizan
voestalpine Stahl GmbH, Austria

Coline Béal, Christof Sommitsch
Graz University of Technology, Austria

ness can be downgauged due to their increased tensile strength, resulting in a significant weight reduction of body structures (4). Furthermore, AHSS are characterized by an improved ductility, which has beneficial impact on the production of complex automotive parts (5). The 1st generation AHSS includes Dual Phase (DP), Transformation-Induced-Plasticity (TRIP) and Complex Phase (CP) steels, with a multiphase microstructure (6,7). These steel grades are already in industrial application, since they are characterized by a good combination of strength and ductility with tensile strengths (UTS) up to 1200 MPa and total elongations (TE) up to 40 % (8,9). The 2nd generation AHSS, which has outstanding mechanical properties with UTS*TE reaching 60,000 MPa%, is represented by Twinning Induced Plasticity (TWIP), Nano-TWIP, Duplex and Triplex steels (10). However, until now, they are hardly used in industrial applications due to their challenging processing and high alloying costs. (11)
Currently, significant effort is put into the development of the 3rd generation AHSS in order to fill the property gap between the 1st and 2nd generation AHSS (12). Therefore, recent research activities focus on the development of Q&P, TBF and medium Mn steels (13,14).

Q&P steels have a microstructure consisting of a carbon-depleted martensitic matrix with a substantial amount of RA (15). Therefore, first the steel is fully austenitized, followed by subsequent quenching to a specific temperature below the M_S temperature in order to adjust the optimal amounts of initial martensite ($\alpha'_{initial}$) and RA. Afterwards, the steel is reheated to the over-ageing region, which triggers the α′ tempering. During this stage the carbide precipitation will be significantly suppressed by the addition of Si and/or Al. This enables the carbon partitioning from α′ into the remaining austenite (γ_{remain}), resulting in its appropriate stabilization to room temperature (RT) upon final cooling (16,17).

Medium Mn steels, which refer to the 3rd generation AHSS, as well, typically contain 3 – 12 wt-% Mn (12). They are characterized by a microstructure consisting of an ultrafine-grained ferritic matrix with typical grain sizes below 1 µm and approximately 30 vol.-% RA (13). Medium Mn steels have excellent mechanical properties with products of R_m*A_{80} exceeding 30,000 MPa% (18).

The combination of the Q&P process and the concept of medium Mn steels resulted in the development of lean medium Mn Q&P steels. (19) In comparison to conventional Q&P steels, this steel grade contains an increased Mn-content (up to 5 wt-%), leading to a larger volume fraction of RA, which is chemically stabilized by C partitioning from α′ to γ_{remain} during isothermal holding in the over-ageing region. The increased amount of RA and the presence of the hard C-depleted martensitic matrix allows for superior performance of these steels in both, deep drawing applications and forming operations such as bending, hole expansion and sheet cutting (20).

By the application of the constrained carbon equilibrium (CCE) model proposed by Speer et al. (21), the amount of RA as a function of T_Q can be predicted. This simplified model allows the calculation of the C-content in γ and therefore the prediction of the volume fraction of RA under three main assumption: (1) full C partitioning from $\alpha'_{initial}$ to γ_{remain}, while the partitioning kinetics are ignored; (2) no movement of phase boundaries during the partitioning process; and (3) no competing reactions like α_B formation or carbide precipitation take place during the Q&P heat-treatment. (21)

According to (22-27), the transformation from γ to αB during isothermal holding at T_P has been observed in several instances.
Clarke et al. (25) and Kaar et al. (26,27) investigated a declining volume fraction of RA due to the formation of carbide-free bainite during the C-partitioning step. However, besides the impact of the bainitic transformation on the amount of RA, an influence on the RA stability was also found (22-24).
This is due to the fact that the formation of carbide-free bainite contributed to the chemical stabilization of RA.

Therefore, the present contribution focusses on the investigation of the transformation behavior of a 0.2C-4.5Mn-1.5Si steel grade. The influence of T_Q and T_P on the transformation kinetics and thus the final microstructure and resulting hardness was investigated in detail. Furthermore, the Q&P

heat-treatment was compared to the TBF process in order to evaluate the influence of the presence of $\alpha'_{initial}$ formed during quenching to T_Q on the IBT.

Experimental Procedure

In the present investigation, a steel grade containing 0.173 wt-% C, 4.46 wt-% Mn, 1.47 wt-% Si and 0.027 wt-% Al was investigated (Table 1). The steel was laboratory fabricated by medium frequency induction melting and cast into an ingot of approximately 80 kg. The material was hot rolled to a thickness of 4 mm, followed by tempering in a batch-annealing-like furnace at 550°C for 16h in order to provide cold rollability. Subsequently, the strip was cold rolled to a thickness of 1 mm. In order to investigate the transformation behavior depending on T_Q and T_P (T_B), a Bähr 805 A/D dilatometer was used. Therefore, specimens with dimensions of 10 x 4 x 1 mm³ were produced by wire-electrical discharge machining.

Tab.2 - Chemical composition of the investigated steel in wt-%

Fe-C-Mn-Si	C	Mn	Si	Al
	0.173	4.46	1.47	0.027

Figure 1 displays the time-temperature regimes for the Q&P (left) and the TBF (right) processes. In both cases, first the samples were fully austenitized at 900°C (T_{an}) for 120 s (t_{an}) using a heating rate HR_1 of 10 K/s. Subsequently, for the Q&P heat-treatment the samples were quenched to various T_Q in the range of 130°C - 290°C in steps of 20°C with a cooling rate CR_1 of 50 K/s. After 10s isothermal holding the samples were reheated with a heating rate HR_2 of 20 K/s to a specific T_P (350, 400 and 450°C) for 600s (t_P). On the contrary, for the TBF cycle after full austenitization, the samples were directly cooled to a T_B of 350, 400 or 450°C and isothermally held for 600s (t_B). Finally, all samples were quenched to RT using a cooling rate CR_2 of 50 K/s.

Microstructural investigations were performed by means of LOM using LePera etching according to (28). Additionally, after electrochemical polishing, SEM was applied for higher resolution examinations.
Mechanical properties were investigated by hardness testing according to Vickers (HV1) using an Emco Test DuraScan 20 device. SMM (29) was used to determine the volume fraction of RA, which was compared to the RA content calculated according to the CCE-model proposed by Speer et al. (21).

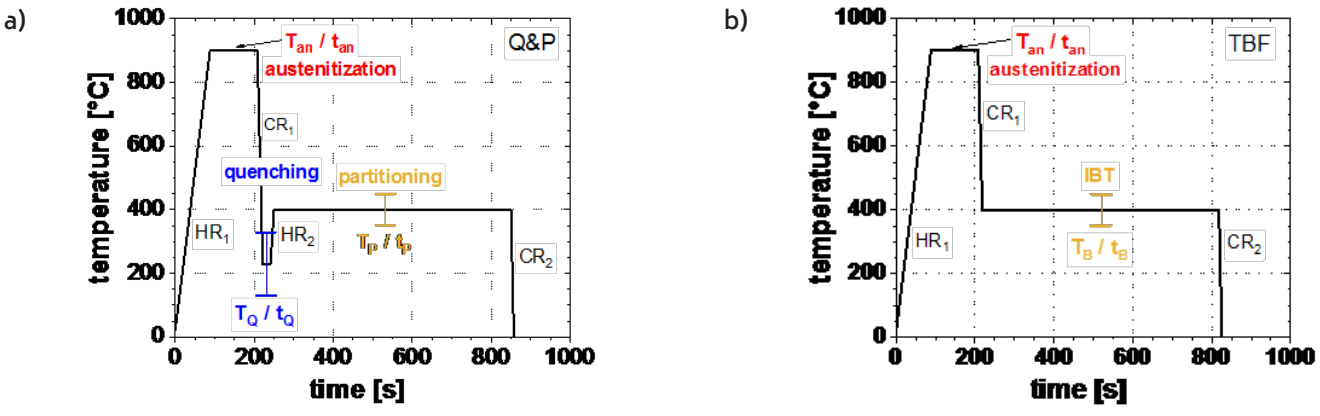

Fig.1 - Time-temperature regimes used for a) the Q&P and b) the TBF heat-treatments (26)

By the application of the Koistinen-Marburger (KM) equation (30), the volume fraction of α′ formed during quenching to T_Q was determined

$$f_M = 1 - e^{(-0.011(M_S - T_Q))} \quad [1]$$

Here, f_M describes the amount of α′ formed during quenching from the γ-region to T_Q. M_S is the martensite start temperature, which was calculated according to Mahieu et al. (31):

$$M_S = 539 - 423C - 30.4Mn - 7.5Si + 30Al \quad [2]$$

Figure 2 a) shows the volume fractions of α′ and γ which were calculated by applying the CCE-model.
Figure 2 b) depicts the related time-temperature regime for the Q&P process. In the CCE-model both, KM- and M_S-equations are applied twice. Initially, the M_S temperature of the γ and the volume fraction of α′ formed during quenching to a specific T_Q (orange line) are calculated.

The remaining amount of γ after quenching is represented by the green curve in Figure 2 a).
Since the applied CCE-model assumes full C partitioning from α′ to remaining γ during isothermal holding at T_P, a new M_S temperature is calculated according to Mahieu.
Given that, the volume fraction of α′ formed during final cooling to RT is calculated (blue line), using the KM equation once again.
The resulting RA content as a function of T_Q is shown in dark green. It is evident that the largest fraction of γ can be retained at that T_Q where no fresh α′ is formed upon final cooling.

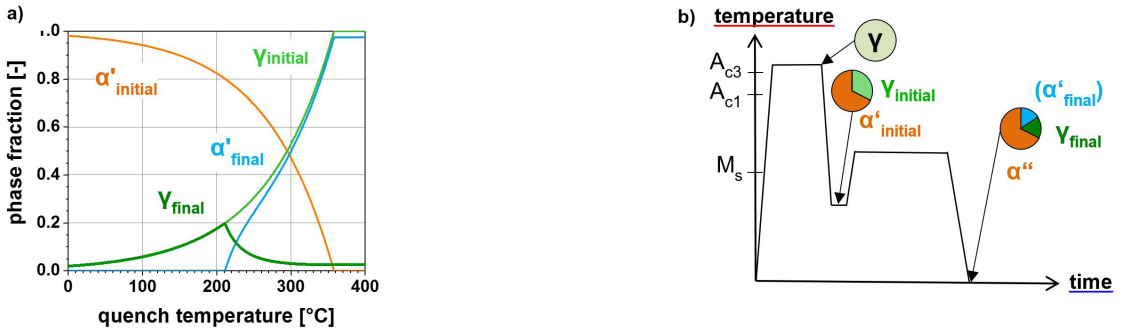

Fig.2 - a) Calculated phase fractions of martensite (α′) and austenite (γ) as a function of T_Q and b) the related Q&P heat-treatment with the schematic microstructural evolution

Results

Transformation Behavior

Figure 3 a) exemplarily shows the influence of T_P on the dilatometric curves for the Q&P samples quenched to a T_Q of 270°C compared to the influence of T_B for the TBF samples (Figure 3 b)). In the case of the Q&P regime, $\alpha'_{initial}$ was formed during quenching to T_Q, since the M_S temperature was approximately 310°C. During isothermal holding at T_P, γ partially transformed to α_B, accompanied by a length expansion apparent from the dilatometer curves. Although the amount of α_B was rather low, an influence of T_P on its phase fraction could be found, since with increasing T_P a smaller length expansion was observed. As a result, T_P indirectly influenced the formation of α'_{final} during cooling to RT: Only for the Q&P samples with a T_P of 350°C the formation of α'_{final} could be fully prevented, whereas at higher T_P of 400 and 450°C the curves confirm the formation of α'_{final} at low temperatures.
On the contrary, for the TBF samples hardly any formation of α_B during isothermal holding at T_B could be observed. The main transformation was the martensitic one during final cooling, indicating that the holding duration of 600 s was definitely too short for bainitizing.

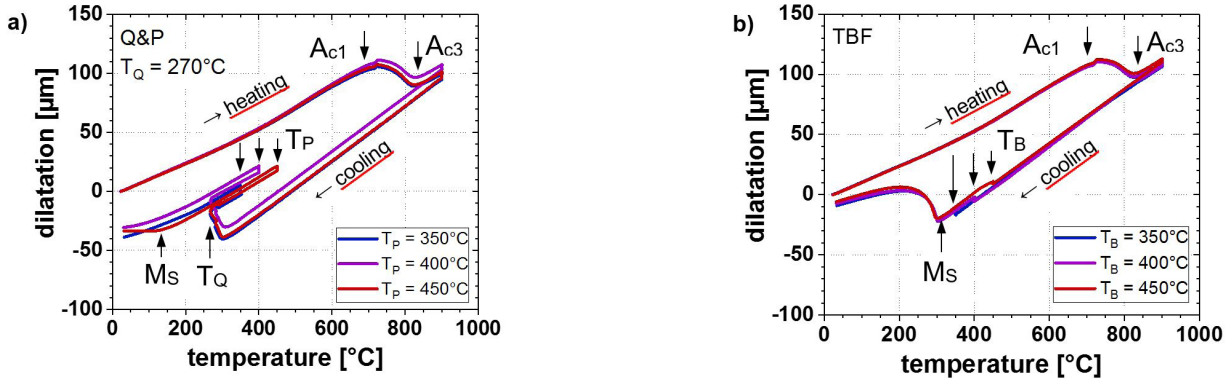

Fig.3 - Dilatometric curves at different T_P (TB) of a) Q&P heat-treatment (T_Q =270°C) and b) TBF heat-treatment

Figure 4 gives a detail view of the influence of T_P and T_B on the α_B formation as a function of isothermal holding time for the Q&P (T_Q = 270°C) and TBF heat-treatment.
In both cases, with increasing T_P and T_B the amount of α_B formed during isothermal holding decreased.
However, especially for a T_P of 350°C and T_B of 350 and 400°C the formation of α_B was not completed during the investigated period of time due to the slower transformation kinetics at lower temperatures.
When comparing the two processes, it is evident that in general for the Q&P samples the larger volume fraction of α_B was formed.

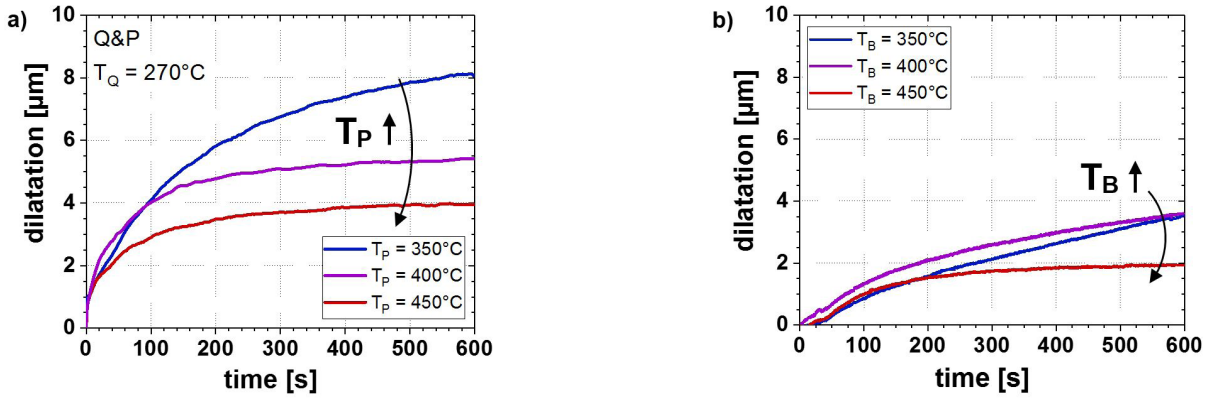

Fig.4 - Dilatation due to α_B formation as a function of isothermal holding time at different T_P (T_B) for a) Q&P heat-treatment (T_Q = 270°C) and b) TBF heat-treatment

In addition, for the Q&P steels the transformation behavior depending on T_Q was investigated (Figure 5).
With increasing T_Q, lower amounts of $\alpha'_{initial}$ were formed due to the lower driving force for the martensite transformation.
On the contrary, the volume fraction of α_B formed during isothermal holding increased with increasing T_Q, which is confirmed by the larger dilatation in Figure 5 b).
Furthermore, as already displayed in Figure 3 a) at very high T_Q of 270°C, the formation of α'_{final} during final cooling to RT was observed.

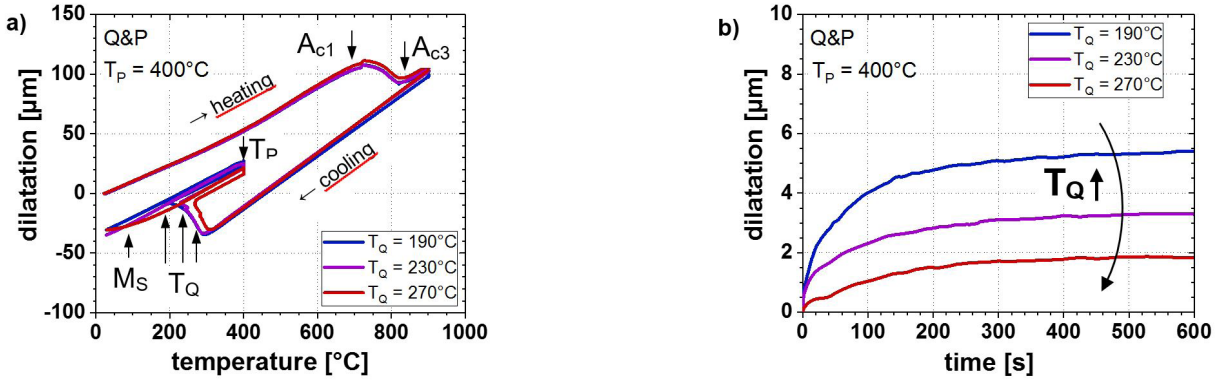

Fig.5 - a) Dilatometric curves at different T_Q (T_P = 400°C) and b) dilatation due to α_B formation as a function of isothermal holding time at different T_Q (T_P = 400°C)

Microstructure

As already confirmed by means of dilatometry, T_Q significantly influenced the phase transformation behavior, and thus, the presence and the amount of the final microstructural constituents of the investigated steel.

Figure 6 a) - c) depicts the LOM images of the Q&P samples quenched to a T_Q of 190, 230 and 270°C, respectively. In comparison, the microstructure of the TBF sample is shown in Figure 6 d). All micrographs relate to the the microstructure obtained at a T_P and T_B of 400°C. The LOM images for the Q&P steels show a matrix consisting of a mixture of α'' and small amounts of α_B, appearing as bluish and brownish areas in the micrographs. Furthermore, RA and/or α'_{final} , represented by the white and brownish areas, could be observed in rising amounts finely distributed in the matrix.

As confirmed by dilatometry, at a T_Q of 190 and 230°C, the secondary phase solely consisted of RA, whereas for the samples quenched to higher T_Q the formation of α'_{final} could not be prevented. On the contrary, the microstructure of the TBF samples primarily consisted of α'_{final} with small amounts of finely distributed RA islands and only small fractions of α_B.

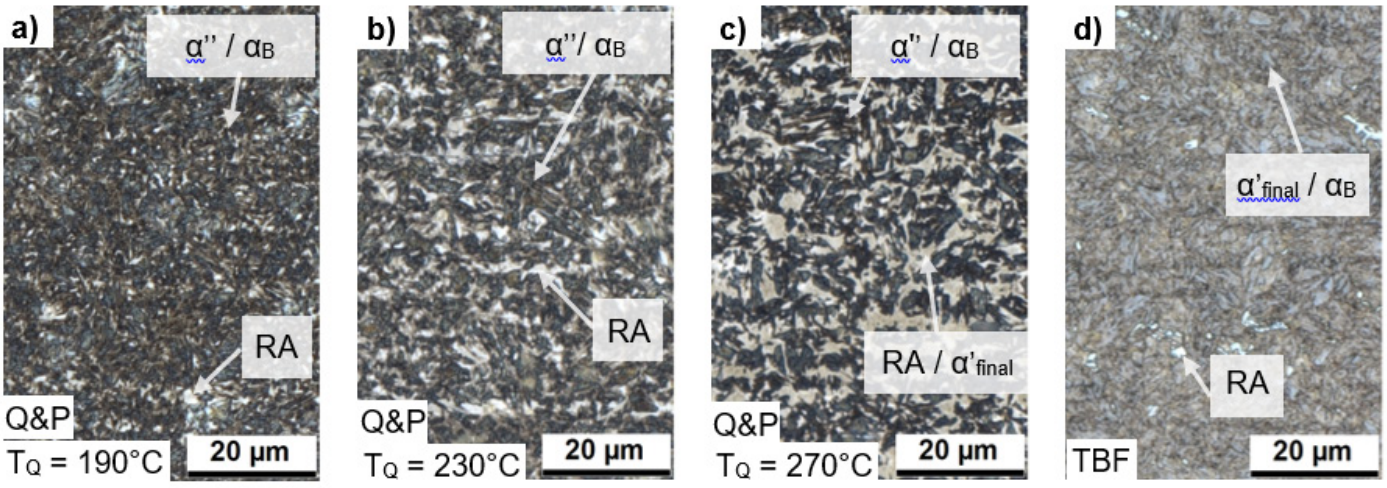

Fig.6 - LOM images of the a) - c) Q&P samples (T_Q = 190, 230 and 270°C) and d) TBF sample at a T_P (T_B) of 400°C (original magnification 1000x)

The SEM images of the Q&P samples quenched to a T_Q of 190, 230 and 270°C are displayed in Figure 7 a) – c), whereas Figure 7 d) depicts the microstructure for the TBF sample. By means of SEM, small amounts of cementite precipitates with an obvious triaxial alignment, confirming the presence of α'', could be observed for the Q&P samples. Concerning the presence of α_B, no significant influence of T_Q was found, since the volume fraction was rather low, independent from T_Q. However, at a T_Q of 270°C a substantial amount of α'_{final} was found in the microstructure. In the present micrographs, RA appears as cavities, since it was dissolved during electrochemical polishing due to its high C and Mn content.
In comparison, the TBF treated sample largely consisted of fine lath like martensite (α'_{final}) with low fractions of RA and α_B.

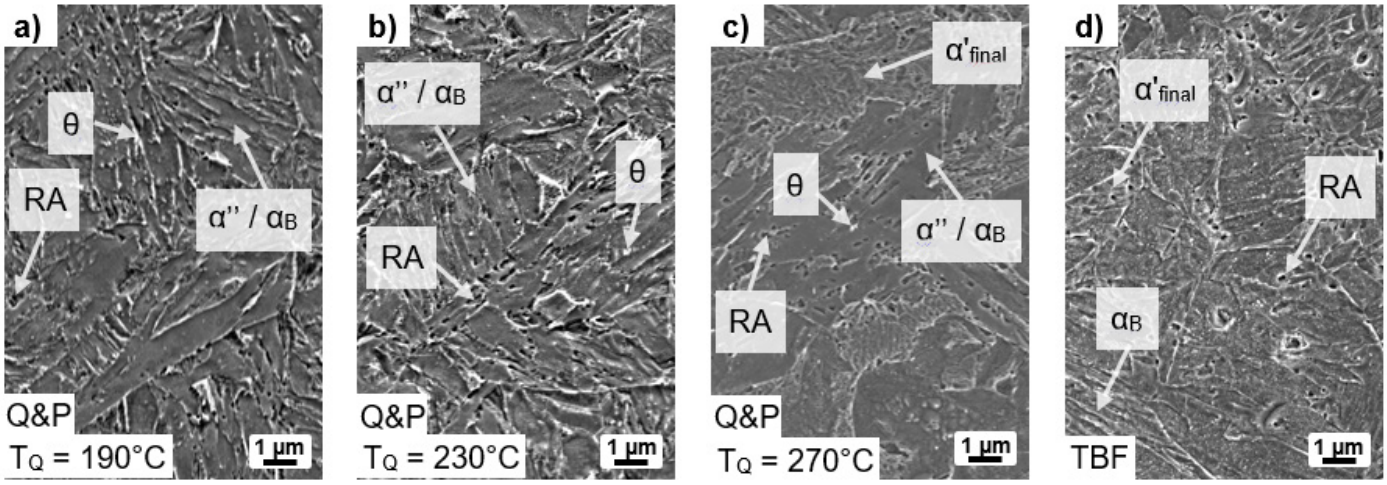

Fig.7 - SEM images of the a) - c) Q&P samples (T_Q = 190, 230 and 270°C) and d) TBF sample at a T_P (T_B) of 400°C (original magnification 5000x)

In Figure 8, the phase fractions in the final microstructure of the Q&P samples are summarized as a function of T_Q for different T_P. In addition, the bar charts, situated close to the right rim of each diagram, depict the microstructural constitution for the steel after TBF treatment. Independent from T_P, for the Q&P samples with increasing T_Q a considerable decrease of α'' was observed, whereas the volume fraction of α_B increased. However, particularly at higher T_Q, a vivid influence of T_P is obvious: the increase of T_P led to a sharply decreasing fraction of α_B, resulting in the formation of α'_{final} upon cooling to RT. Therefore, the RA content steadily rose with increasing T_Q until the onset of the formation of α'_{final} occured. For the TBF samples, it is obvious that only small amounts of α_B were formed at all investigated temperatures as already shown by dilatometry (Figure 4 b). Due to these low α_B fractions, the largest amount of γ transformed into α'_{final} during final cooling, in turn resulting in comparably low amounts of RA.

In Figure 9, the amount of RA measured by means of SMM is plotted in detail as a function of T_Q at a T_P of 350, 400 and 450°C. Furthermore, the volume fraction of RA for the TBF treated samples is shown in the form of dotted lines. In addition, the diagram contains the calculated RA fraction according to the CCE-model. This model proposed a RA maximum (RA_{max}) of 19.8 vol.-% at a T_Q of 173°C. In accordance with the model calculations, the experiments also confirmed the fundamental shape of the RA evolution as a function of T_Q. At very low T_Q large amounts of $\alpha'_{initial}$ were formed, leading to low RA fractions. With increasing T_Q the amount of $\alpha'_{initial}$ decreased, and therefore the volume fraction of RA increased, until RA_{max} was achieved, followed by a decline in RA content. This decreasing amount of RA at higher T_Q was due to the lower chemical stabiliza-

tion of austenite and the resulting formation of α'_{final} upon cooling to RT. The experiments further show an influence of T_P on the volume fraction of RA: by increasing T_P from 350 to 400°C, RA_{max} rose from 19.7 to 22.4 vol.-%.
In this context, at the T_P of 350°C, the amount of RA correlated well with the model calculations. On the contrary, at the T_P of 400°C and 450°C, a higher amount of RA was achieved compared to the model predictions. Moreover, RA_{max} occurred for all T_P, at temperatures 60 to 70°C higher than predicted by the CCE-model.
It is evident that the RA contents determined for the TBF samples were much lower compared to the Q&P samples, ranging from 4.6 vol.-% RA at a T_B of 450°C to 7.1 vol.-% RA at T_B = 350°C.

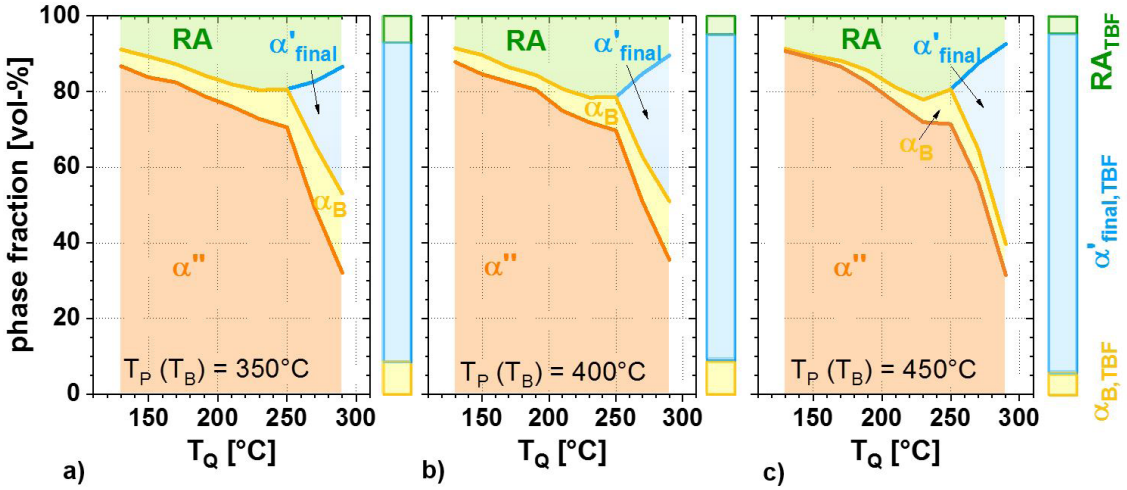

Fig.8 - Phase fraction as a function of T_Q for a T_P (TB) of a) 350°C, b) 400°C and c) 450°C

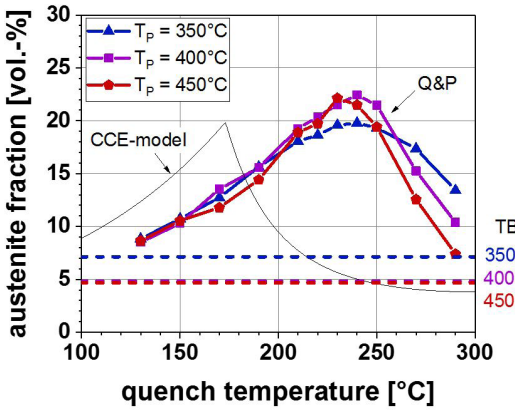

Fig.9 - RA content as a function of T_Q for a T_P (T_B) of 350, 400 and 450°C

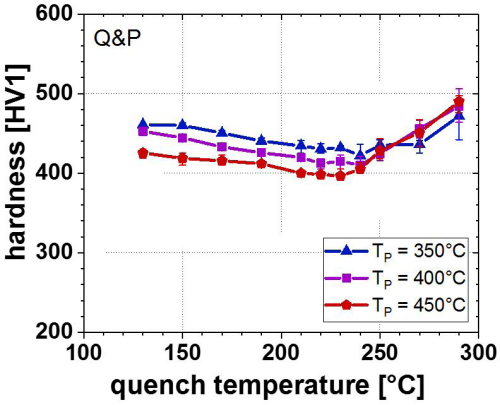

Fig.10 - Vickers hardness as a function of T_Q for a T_P of 350, 400 and 450°C

Hardness

Figure 10 depicts the hardness according to Vickers as a function of T_Q. In the T_Q range of 130 to 230°C, both increasing T_Q and T_P led to a slight decrease in hardness. However, when further increasing T_Q, a considerable increase in hardness could be observed, especially at a T_P of 450°C. For this reason, in the case of the Q&P samples, the hardness was between approximately 400 and 500 HV1. In contrast, for the TBF samples hardness was quite constant with 510 HV1 at a T_B of 400°C, and 511 HV1 at 350 and 450°C, respectively.

Discussion

In Figure 11, the IBT for the Q&P samples (exemplarily at a T_Q of 270°C) and the TBF samples is compared. The TTT diagrams show an evident acceleration of the α_B formation in case of the Q&P process. This is in agreement with Kaar et al. (26) and Wang et al. (32), since the presence of $\alpha'_{initial}$ pronouncedly accelerated the IBT due to the presence of geometrically necessary dislocations, acting as nucleation sites for the α_B formation. When comparing the IBT of the present steel grade with that of a Fe-C-Mn-Al steel investigated in (26), it is evident that the substitution of Si by Al leads to a larger amount of α_B formed during isothermal holding at T_P. According to (33) this can be explained by the fact that Al shifts the T_0-line to higher C-contents, enabling the formation of a larger amount of α_B.

Furthermore, in the present case, a general impact of the T_P (T_B) on the transformation kinetics was found: especially at a T_P (T_B) of 400°C, the transformation kinetics was evidently accelerated due to the faster C diffusion into the remaining γ, while at 450°C a reduced driving force for the bainitic transformation seems to limit the transformation kinetics.

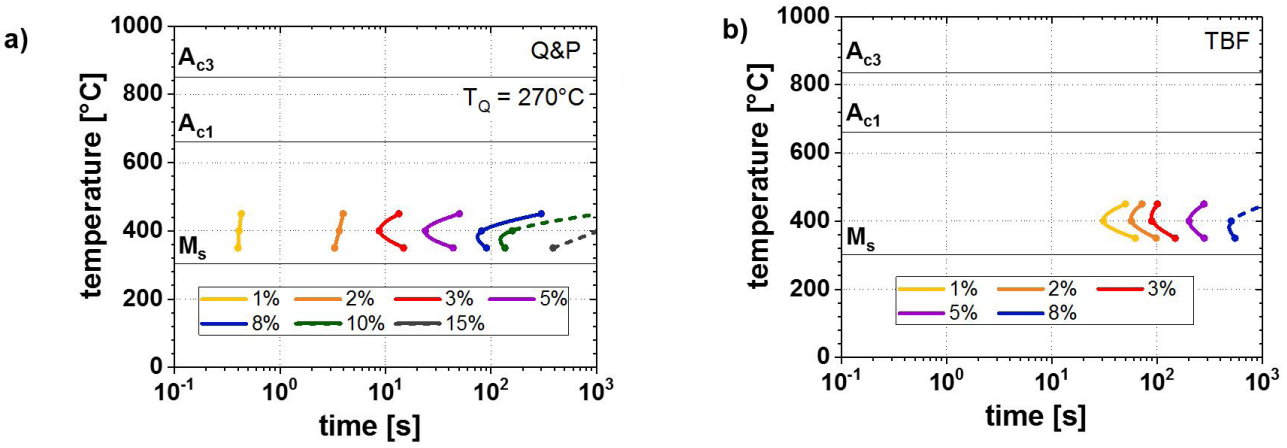

Fig.11 - TTT diagrams for a) Q&P steels (T_Q = 270°C) and b) TBF steels

Furthermore, in terms of RA investigations, a considerable difference between the calculated CCE-model and experimental data was found. This was particularly apparent for the amount of RA and optimal T_Q, which is in agreement with results reported in literature (21,26,27,34). One reason for this discrepancy is the fact that the application of the CCE-model assumes full C-partitioning from $\alpha'_{initial}$ into the remaining γ. However, in the present case, the presence of cementite was observed in the microstructure (Figure 7), which contradicts this assumption. This led to both, a lower amount and chemical stability of γ_{remain}, resulting in the formation of α'_{final} during cooling to RT and thus lower RA contents. Furthermore, the CCE-model does not consider the formation of α_B, associated with a decline in RA content. In comparison to the Fe-C-Mn-Al steel grade investigated in (26,27), the RA content was higher for the Si-alloyed steel examined in this contribution due to the lower amount of α_B formed during isothermal holding. This indicated that in the present case, RA was mainly stabilized via C-partitioning during the partitioning step, whereas for the Al-alloyed steel investigated in (26, 27) the RA stabilization was achieved by both, formation of α_B and C-partitioning.

In general, in terms of RA stability, both, chemical and mechanical stabilization have to be considered (35). However, the CCE-model only takes into account the chemical stabilization, which explains the significant shift of the RA_{max} to higher T_Q than predicted. Additionally, two empirical formulas, describing the α' kinetics and the M_S temperature, are included in the CCE-model. Therefore, slight differences in the chemical composition due to segregations could lead to deviations from the model, as well (36). Nevertheless, the CCE-model proposed by Speer et al. (21) is a vital tool for the first estimation of applicable annealing parameters in case of Q&P steels.

Conclusions

The results of the present investigation indicate that the Q&P process has significant influence on the transformation behavior of lean medium Mn steels.

It is of vital importance to carefully set both, T_Q and T_P, since they have significant impact on the microstructural constituents and thus, certainly mechanical properties.

The main findings of the present contribution can be summarized as follows:

• In case of the Q&P process, the formation of $\alpha'_{initial}$ during quenching to T_Q significantly accelerated the IBT, acting in the form of vital nucleation sites.

• For both, Q&P and TBF processes, with increasing T_P (T_B) the IBT kinetics was accelerated, but the amount of α_B formed during isothermal holding was decreased.

• The increase in T_Q resulted in a lower volume fraction of $\alpha'_{initial}$ and slightly larger amounts of α_B. Therefore, the volume fraction of RA increased, until that T_Q where α'_{final} was formed and thus RA content declined sharply. In case of the Q&P samples this led to a final microstructure consisting of α'', RA and at higher TQ partially of α_B and α'_{final}.

• Especially for the Q&P samples heat-treated at a low T_P, the comparison of the CCE-model and the experimental data showed a significant divergence in terms of RA content. Additionally, a substantial shift of the RA-maximum to higher T_Q was observed compared to the CCE-model predictions.

• In the present case, for the Si-alloyed steel grade RA was mainly stabilized by C-partitioning during isothermal holding at T_P, whereas on the contrary for the Al-alloyed steel investigated in (26, 27), the RA stabilization was performed by both, formation of α_B and simultaneous C-partitioning.

Acknowledgements

The authors sincerely acknowledge the support of the Austrian Research Promotion Agency (FFG) related to the frontrunner project No. 860188 "Upscaling of medium Mn-TRIP steels".

References

[1] Kwon O, Lee K, Kim G, Chin K. New trends in advanced high strength steel - developments for automotive application. Mater. Sci. Forum. 2010:638-642:136-141.

[2] Spenger F, Hebesberger T, Pichler A, Krempaszky C, Werner E, Doppler C. AHSS steel grades: strain hardening and damage as material design criteria. Proc. Int. Conf. on New Developments in AHSS. 2008 Jun. 15-18; Orlando, USA. p. 39-49.

[3] Jacques P, Petein A, Harlet P. Improvement of mechanical properties through concurrent deformation and transformation: new steels for the 21st century. Proc. Int. Conf. on TRIP-aided high strength ferrous alloys. 2002 Jun. 19-21; Aachen, Germany. p. 281-285.

[4] Hashimoto K, Yamasaki M, Fujimura K, Matsui T, Izumiya K. Global CO2 recycling - novel materials and prospect for prevention of global warming and abundant energy supply. Mater. Sci. Eng. A. 1999:267:2:200-206.

[5] Zaefferer S, Ohlert J, Bleck W. A study of microstructure, transformation mechanisms and correlation between microstructure and mechanical properties of a low alloyed TRIP steel. Acta Mater. 2004:52:2765-2778.

[6] Matlock D, Speer J, De Moor E, Gibbs P. Recent developments in advanced high strength steels for automotive applications: an overview. JESTECH. 2012:15:1-12.

[7] De Cooman BC. Structure-properties relationship in TRIP steels containing carbide-free bainite. Solid State Mater. Sci. 2004:8:285-303.

[8] Hairer F, Krempaszky C, Tsipouridis P, Werner E, Satzinger K, Hebesberger T, Pichler A. Effects of heat treatment on microstructure and mechanical properties of bainitic single- and complex-phase steel. Proc. of MS&T. 2009 Oct. 25-29; Pittsburgh, USA. p. 1391-1401.

[9] Samek L, Krizan D. Steel - Material of choice for automotive lightweight applications. Proc. Int. Conf. Metal 2012. 2012 May 23-25; Brno, Czech. p. 6-12.

[10] De Cooman BC, Chin K, Kim J. High Mn TWIP steels for automotive applications. Chapter 6 in: New trends and developments in automotive system engineering. M. Chiaberge (ed.), DOI: 10.5772/14086.

[11] Bracke L, Verbeken K, Kestens L, Penning J. Microstructure and texture evolution during cold rolling and annealing of a high Mn TWIP steel. Acta Mater. 2009:57:1512-1524.

[12] Steineder K, Schneider R, Krizan D, Béal C, Sommitsch C. Microstructural evolution of two low-carbon steels with a medium manganese content. Proc. of 2. HMnS Conf. 2014 Aug. 31 – Sept. 4; Aachen, Germany. p. 351-354.

[13] Steineder K, Schneider R, Krizan D, Béal C, Sommitsch C. On the microstructural characteristics influencing the yielding behavior of ultra-fine grained medium-Mn steels. Acta Mater. 2017:139:39-50.

[14] De Cooman BC, Speer J. Quench and partitioning steel: A new AHSS concept for automotive anti-intrusion applications. Steel Res. Int. 2006:77:634-640.

[15] Speer J, Matlock D, De Cooman BC, Schroth J. Carbon partitioning into austenite after martensite transformation. Acta Mater. 2003:51:2611-2622.

[16] Speer J, Aussunção F, Matlock D, Edmonds D. The quenching and partitioning process: Background and recent progress. Mat. Res. 2005:8:4:417-423.

[17] Edmonds D, He K, Rizzo F, De Cooman BC, Matlock D, Speer J. Quenching and partitioning martensite - A novel steel heat treatment. Mater. Sci. Eng. A. 2006:438-440:25-34.

[18] Arlazarov A, Gouné M, Bouaziz O, Hazotte A, Petitgand G, Barges P. Evolution of microstructure and mechanical properties of medium Mn steels during double annealing. Mater. Sci. Eng. A. 2012:542:31-39.

[19] De Moor E, Lacroix S, Clarke A, Penning J, Speer J. Effect of retained austenite stabilized via quench and partitioning on the strain hardening of martensitic steels. Metall. Mater. Trans. A. 2008:39A:2586-2595.

[20] Huyghe P, Dépinoy S, Caruso M, Mercier D, Georges C, Malet L, Godet S. On the effect of Q&P processing on the stretch-flange-formability of 0.2C Ultra-high Strength Steel. ISIJ Int. 2018:58:1341-1350

[21] Speer J, Streicher A, Matlock D, Rizzo F. Quenching and partitioning: a fundamentally new process to create high strength TRIP sheet microstructures. Austenite formation and decomposition. 2003:505-522.

[22] Van Bohemen S, Santofimia M, Sietsma J. Experimental evidence for bainite formation below Ms in Fe-0.66C. Scr. Mater. 2009:58:488-491.

[23] Somani M, Porter D, Karjalainen L, Misra R. On various aspects of decomposition of austenite in a high-silicon steel during quenching and partitioning. Metall. Mater. Trans. A. 2013:45A:1247-1257.

[24] Kim D, Speer J, De Cooman BC. Isothermal transformation of a CMnSi steel below the Ms temperature. Metall. Mater. Trans. A. 2011:42a:1575-1585.

[25] Clarke A, Speer J, Miller M, Hackenberg R, Edmonds D, Matlock D, Rizzo F, Clarke K, De Moor E. Carbon partitioning to austenite from martensite or bainite during the quench and partition (Q&P) process: A critical assessment. Acta Mater. 2008:56:16-22.

[26] Kaar S, Schneider R, Krizan D, Béal C, Sommitsch C. Influence of the Quenching and Partitioning Process on the Transformation Kinetics and Hardness in a Lean Medium Manganese TRIP Steel. Metals. 2019:9:353:1-13

[27] Kaar S, Schneider R, Krizan D, Béal C, Sommitsch C. Influence of the phase transformation behaviour on the microstructure and mechanical properties of a 4.5 wt-% Mn Q&P steel." HTM J. Heat Treatm. Mat. 2019:74:2:70-84.

[28] Zakerinia H, Kermanpur A, Najafizadeh A. Color metallography: a suitable method for characterization of martensite and bainite in multiphase steels. Int. J. ISSI. 2009:6:1:14-18.

[29] Technical Report: Vatron GmbH, Restaustenit Magnetjoch – Neue Erkenntnisse und Möglichkeiten. 2009

[30] Koistinen D, Marburger R. A general equation prescribing the extent of the austenite-martensite transformation in pure iron-carbon alloys and plain carbon steels. Acta Metall. 1959:7:59-60.

[31] Mahieu J, Maki J, De Cooman BC, Claessens S. Phase transformation and mechanical properties of Si-free CMnAl transformation-induced plasticity-aided steel. Metall. Mater. Trans. A. 2002:33:8:2573-2580.

[32] Wang G, Chen S, Liu C, Wang C, Zhao X, Xu W. Correlation of isothermal bainite transformation and austenite stability in quenching and partitioning steels. J. Iron Steel Res. Int. 2017:24:1095-1103.

[33] Bhadeshia HKDH, Honeycombe R. Steels - Microstructure and properties, 3rd edition. 2006:ISBN-13: 978-0-750-68084-4.

[34] Steineder K, Schneider R, Krizan D, Béal C, Sommitsch C. Investigation on the microstructural evolution in a medium-Mn steel (X10Mn5) after intercritical annealing. HTM J. Heat Tr. Mat. 2015:70:19-25.

[35] Jimenez-Melero E, van Dijk N, Zhao L, Sietsma J, Offerman S, Wright J, van der Zwaag S. Martensitic transformation of individual grains in low-alloyed TRIP steels. Scr. Mater. 2007:56:421-424.

[36] Kim S, Lee J, Barlat F, Lee MG. Transformation kinetics and density models of quenching and partitioning (Q&P) steels. Acta Mater. 2016:109:394-404.